Enhanced Mechanical, Anticorrosion, and Antimicrobial Properties of Epoxy Coating *via* Pine Pollen Modified Clay Incorporation

Edraki, Milad
Polymer Department, Technical Faculty, South Tehran Branch, Islamic Azad University, Tehran, I.R. IRAN

Sheydaei, Milad*+
Faculty of Polymer Engineering, Sahand University of Technology, Tabriz, I.R. IRAN

Vessally, Esmail
Department of Chemistry, Payame Noor University, Tehran, I.R. IRAN

Salmasifar, Amir
Polymer Department, Technical Faculty, South Tehran Branch, Islamic Azad University, Tehran, I.R. IRAN

ABSTRACT: *In this study, Pine Pollen (PP) was introduced into the structure of sodium montmorillonite (Na^+-MMT), and then these new nanoparticles (PP-MMT) were added to the Epoxy Resin (EP), and new nanocomposites were prepared. The results of the PP-MMT investigation confirmed the presence of PP in the structure. The results of polarization and salt spray tests showed that the presence of PP-MMT in the matrix improves corrosion resistance, so the coating containing 1.5wt. % PP-MMT showed an inhibition efficiency of about 87%. The storage module (E') for EP was 2170 MPa, which increases with increasing PP-MMT content up to 2350 MPa, also the effect of PP-MMT on the glass transition temperature (T_g) was up to 2.5 °C. Also, the strength and Young's modulus increased up to 13 and 126 MPa, respectively. Moreover, the antimicrobial results showed that the presence of PP-MMT made the nanocomposite effective against Bacillus subtilis, Staphylococcus epidermidis, Escherichia coli, and Shigella dysenteriae.*

KEYWORDS: *Epoxy resin; Pine pollen; Dynamic mechanical analysis; Corrosion; Antimicrobial.*

INTRODUCTION

Corrosion is an important issue that can be triggered by natural or manmade activities and reduce the strength and quality of metallic and metal-based alloys [1-3]. Different methods are used to protect metals and reduce their corrosion rate, of which the use of polymer coatings is one of the most important [4]. Meanwhile, EPs are that high-

**To whom correspondence should be addressed.*
+ E-mail: mi_sheydaei@sut.ac.ir , m.sheydaei@yahoo.com
1021-9986/2023/9/2875-2886 13/$/6.03

Table 1: Percentages of the elements present in the mild steel

Element	Fe	C	Si	Mn	P	S	Al
wt.%	99.01	0.19	0.34	0.32	0.05	0.05	0.04

performance polymer coatings that were prepared in 1909 are actually low molecular-weight pre-polymers [5,6]. EPs are in the group of thermoset resins and are cured with different types of curing agents. The final properties of the product depend on the specific combination of EPs and curing agents [7]. EPs have excellent mechanical properties, strong adhesion for many substrates, dimensional stability, and suitable heat and chemical resistances [8,9]. Therefore, they can be used in different applications such as structural adhesives, electrical insulation, coatings, and injection molding materials [10,11]. Also, EPs are highly compatible with polysulfide polymers [12-20]. Moreover, nanofillers such as clay and graphene can be used to improve the properties of polymer coatings [21-22]. On the other hand, the high resistance of many bacteria and fungi is relatively worrying issue [23,24]. Over the years, one of the biggest advances has been antimicrobial materials because they can be used in hospitals and crowded environments [25]. Therefore, it is very important to use a cover that can be effective in all fields. Today, one of the important issues is the use of non-toxic, cost-effective, and environmentally friendly materials [26]. Hence, PP is a remarkable particle because it has anti-corrosive and antimicrobial effects due to its richness in important compounds such as proteins, amino acids, lipids, flavonoids, nucleic acids, and saccharides [27-29]. *Dehghani et al*. [30] loaded the benzimidazole inhibitor within a β-Cyclodextrin (β-CD) reservoir and used it as an anti-corrosion additive in silane (sol-gel) coatings to protect mild steel in a corrosive saline medium. Due to the controlled release of the inhibitor from the reservoir, the corrosion of mild steel decreased by about 84%. *Dong et al*. [31] inserted the 2-mercaptobenzothiazole inhibitor inside the interlayer space of layered double hydroxide anionic clay. After that, it was dispersed as an anti-corrosion nanopigment in an epoxy polymeric matrix and was afterward on a steel sample. SEM images clearly showed that after 13 h of immersion in the electrolyte solution, the epoxy coating containing nanopigment filled the scratch due to the release of 2-mercaptobenzothiazole from the layered double hydroxide nanocapsule that resulted in the healing of this coating. Here, we prepared new nanocomposites using PP-MMT and EP and investigated their anti-corrosion, mechanical, adhesion and antimicrobial properties.

EXPERIMENTAL SECTION

Materials

The sodium montmorillonite nano clay was obtained from Rockwood Company (USA). Epoxy resin (Bisphenol A diglycidyl ether) and jeffamine D230 (Curing agent) were obtained from Taak Resin Kaveh Company (Iran). Methyl ethyl ketone and xylene were purchased from Merck Chemicals Co. (Germany). Moreover, pine (*Picea abies*) pollen was collected from Lajim forest (Savadkuh city, Iran). The substrates used were made of mild steel with dimensions of 5 cm × 10 cm, which were purchased from the Iranian Mobarakeh Steel Company in Isfahan. The elemental analysis of this mild steel is presented in Table 1. To prepare the surface, the steel plates were mechanically polished by corundum papers ranging from 600 to 1200 grades then cleaned using acetone.

Modification of Na^+-MMT by PP

To begin the modification, the Na^+-MMT was first swollen [32]. For this purpose, Na^+-MMT (10 g) was added to distilled water (700 mL, 25 °C) and stirred for 24 h. Next, PP (4 g) was added to distilled water (200 mL, 25 °C), stirred for 2 h and added to the previous mixture. The mixture containing Na^+-MMT and PP was stirred at room temperature (25 °C) for 24 h and then the mixture was allowed to rest for 24 h. Finally, PP-MMT was obtained by centrifuging the mixture (for 15 min at 5000 rpm) and was vacuum-dried (for 24 h at 30 °C).

Preparation of EP/PP-MMT nanocomposite

To prepare the nanocomposites, PP-MMT and a solvent mixture (to reduce the viscosity of resin) containing xylene and methyl ethyl ketone (the ratio was 1:1) were added to bisphenol A diglycidyl ether. Then, the mixture was stirred for 45 min (by mechanical stirrer at 3000 rpm). Next, jeffamine D230 was added to the mixture (the ratio of hardener to resin was 1:2) and mixed for 3 min. Then, the mixture was cast coated on the mild steels with a thickness of 100 μm. The samples were kept up at ambient temperature for 7 days and after that placed in an oven at 60°C for 1 h. Finally, the dry film thickness of 55 μm was obtained. The PP-MMT content in the nanocomposites was

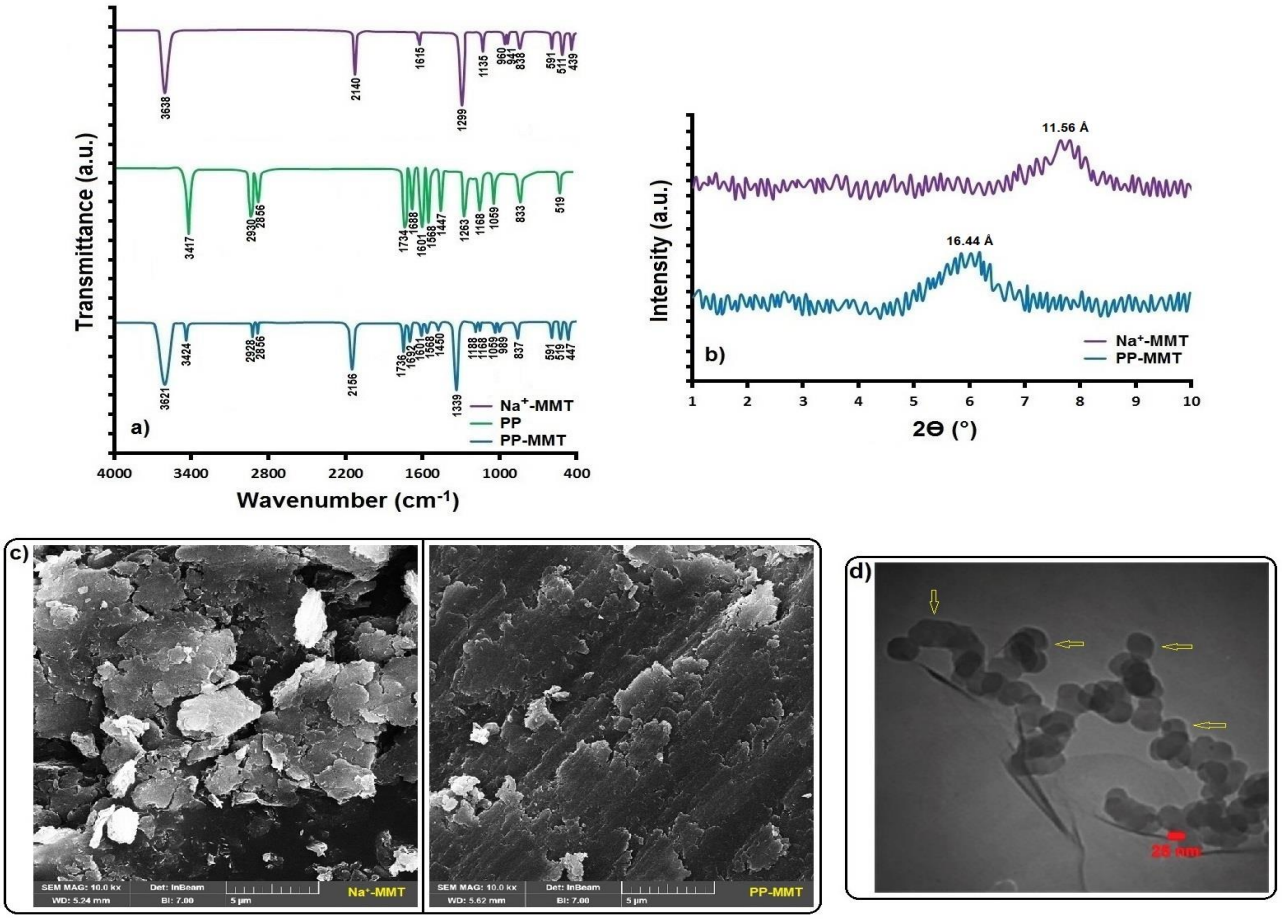

Fig. 1: (a) FT-IR spectra of Na^+-MMT, PP, and PP-MMT, (b) XRD patterns of Na^+-MMT and PP-MMT, (c) SEM images of Na^+-MMT and PP-MMT, and (d) TEM images of PP-MMT

0.5, 1,and 1.5 *wt*. %. A sample without PP-MMT was also prepared.

The measurements and characterization

Fourier Transform InfraRed (FT-IR) was a Equinox 55 spectrometer (Bruker, Germany). Xpert Pro MPD diffractometer (Panalytical, Netherlands) was used for X-Ray Diffraction (XRD) measurements. EDS combined with Scanning Electron Microscopy (SEM) (SEM-EDX) was performed on a Cambridge apparatus. SEM images were provided using a S4160 (Hitachi, Japan). The Transmission Electron Microscope (TEM) was a Philips CM10 (Netherlands). The adhesion strength was investigated by a pull-off adhesion tester (PosiTest AT-M, Defelsko, USA), and three repeats were performed per each sample. The film thickness was investigated by Elcometer A456CFBI1 (United Kingdom, 0-1500µm, Ferrous). The friction properties were measured using the friction-wear tester (UMT-2MT, Bruker, Germany). Also, the friction coefficients were tested upon friction with a GCr15 stainless steel ball with 3 mm in diameter for 30 min (under a 5 N load at 5 Hz friction frequency). Dynamic mechanical analysis (DMA) was a NETZSCH DMA 242C (Netherlands). The frequency was 1 Hz and the range was -20 to 180 °C. A tensile test of the samples (five repeats for each sample) was performed on Hiva 200 (Hiva, Iran) at a speed of 10 mm min^{-1} (ASTM D-2370). Salt spray tests were carried out for samples on a S83-V300 cabin test (Pars Horm, Iran) at 40 °C (pH: 7) according to ASTM B117. To prevent rusting, the back and edges of substrates were covered *via* a mixture of Beeswax melt and colophony resin with a ratio of 2.5 to 1. Also, scratches 0.5 mm thick were made on the coatings using Elcometer 1538 (United Kingdom). The polarization measurements were executed in an electrochemical cell (platinum as counter and Ag/AgCl as reference), and coated samples with an exposed

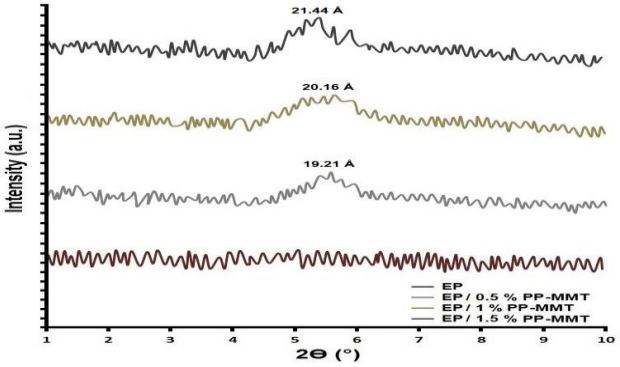

Fig. 2: XRD patterns of samples

area of 1 cm^2 (as working) electrodes in brine solution after 30 days of immersion. This analysis was performed using a AUTOLAB PGSTAT 302N (Switzerland). The data collection was accomplished thoroughly from beneath 200 mV to over 200 mV of the open circuit potential (E_{ocp}) at a scanning rate of 0.5 mV/s. Tafel plots were analyzed meticulously with the aim of acquiring the polarization resistance (R_p) considering Stern Geary equation (Eq. (1)) [33,34].

$$R_P = \frac{\beta_a . \ \beta_c}{2.303(\beta_a+\beta_c)} \times \frac{1}{I_{corr}} \quad (1)$$

In the mentioned equation, the anodic Tafel slope, cathodic Tafel slope, and the corrosion current density are β_a, β_c, and I_{corr}, respectively. Also, the Corrosion Rate (C.R) was also calculated *via* Eq. (2) [35].

$$C.R = \frac{0.0032 \ \ I_{corr} \ \ MW}{nd} \quad (2)$$

In the mentioned equation, corrosion current density (µA/cm^2), molar mass (g/mol), charge number, and density (g/cm^3) of the tested metal are I_{corr}, *MW*, *n*, and *d*, respectively. The percentage Inhibition efficiency (*IE%*) for each EP/PP-MMT nanocomposite coatings was calculated using Eq. (3) [36].

$$IE(\%) = \frac{I_{corr\ (neat\ coating)} - I_{corr\ (nanocomposite\ coating)}}{I_{corr\ (neat\ coating)}} \times 100 \quad (3)$$

Where, $I_{corr\ (neat\ coating)}$ and $I_{corr\ (nanocomposite\ coatings)}$ are the corrosion current densities of coatings without and with the PP-MMT, respectively.

Antimicrobial test

Antibacterial properties were investigated through the agar diffusion method as described in the literature [37], and the Minimum Inhibitory Concentration (MIC) and Minimum Bactericidal Concentration (MBC) were also investigated.

RESULTS AND DISCUSSION

Fig. 1 shows the results for the PP-MMT modification investigation. As shown in the FTIR results (in Na^+-MMT), the peaks at around 439 and 1135-1299 cm^{-1} correspond to the Si-O vibration [38,39]. Also, the peaks appeared around 511, 591, 839, and 941-960 cm^{-1} are corresponded to those in SiOAl and MgO vibration groups, FeOSi or MgOSi groups, AlMgOH vibration groups, and Al_2OH bending groups, respectively [39,40]. Moreover, peaks at around 1615-2140 and 3638 cm^{-1} are attributed to scissoring vibrations and symmetric vibrations of OH units and stretching of OH (SiOH groups) [40,41]. In PP spectrum, peaks at around 2856-2930 and 1734 cm^{-1} are attributed to stretching vibrations of CH_2 groups and stretching vibrations of C=O groups (the absorptions of lipids) [42]. The peaks at around 1568 and 1601-1688 cm^{-1} are corresponding to the N-H bending inside (protein (amide II)) and C=O stretching (protein (amide I)) [42,43]. Also, the peak at around 3417 cm^{-1} is related to the hydroxyl absorption of polysaccharides [39,40]. Moreover, the peaks at around 519, 833, 1059-1168, 1263, and 1447 cm^{-1} correspond to those in the skeletal mode (glucan), C-H vibrations (polysaccharides), C-C vibrations (polysaccharides), CH_2OH vibrations (polysaccharides), and CH_2 vibrations (polysaccharides), respectively [39,42]. Finally, PP and Na^+-MMT peaks are observed in the PP-MMT spectrum. XRD results show that Na^+-MMT has a peak at $2\theta = 7.9°$ (*d*-spacing = 11.56 Å) and PP-MMT has a peak at $2\theta = 5.9°$ (*d*-spacing = 16.44 Å). As the results show, after modification 2θ and *d*-spacing change in the samples, which is due to the presence of PP and also the absence of Na^+ cation, which increases the MMT interlayer space. As the SEM images show before and after modification, the structure is plate and the morphology does not change significantly, which this behavior has been reported in the literature [44]. But, the TEM image (Fig. 1(d)) clearly shows that PP particles are located between the MMT plates. According to the results, it can be said that the exchange of Na^+ cations with PP has been successful.

XRD patterns were used to study the effect of PP-MMT on the structure (see Fig. 2). The results showed that EP lack a peak, but nanocomposites have a peak due to the presence of PP-MMT (see XRD discussion of PP-MMT).

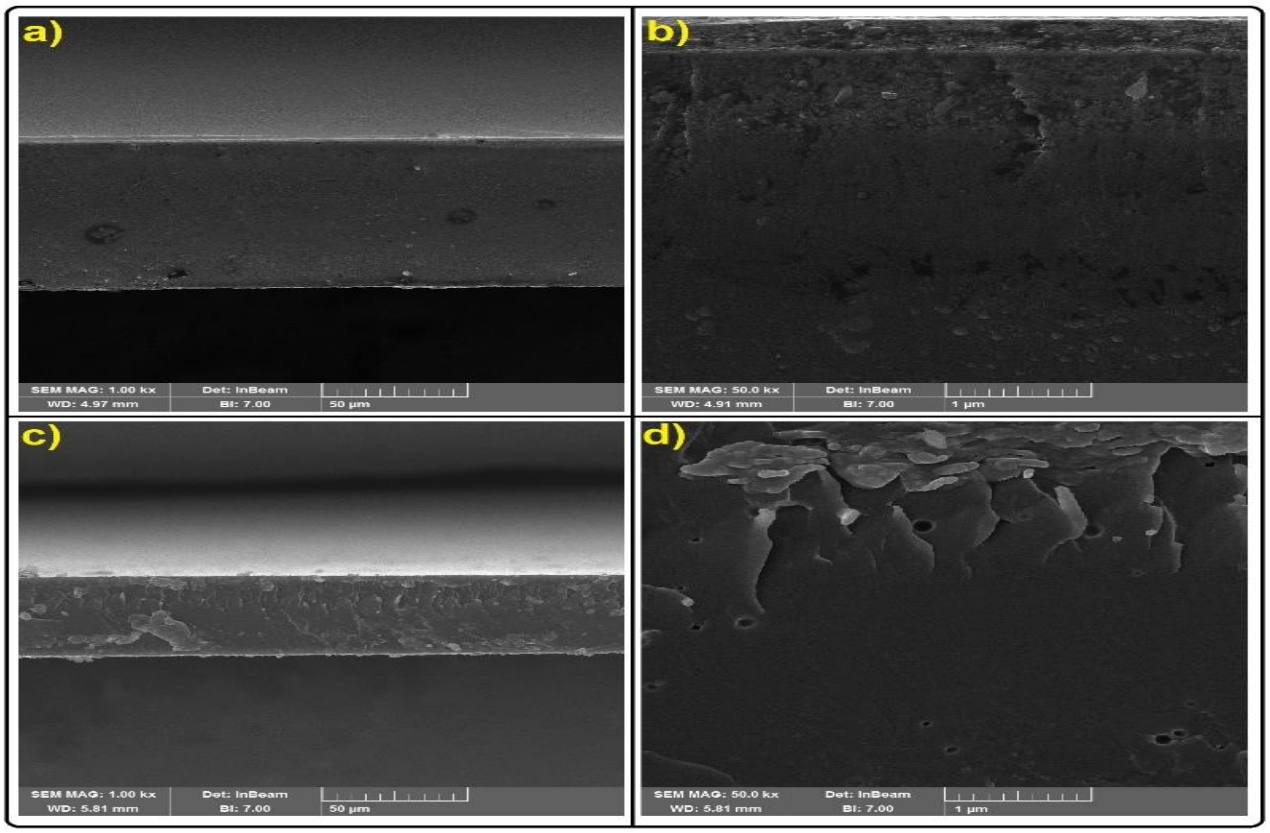

Fig. 3: SEM images of (a- b) EP, (c- d) EP / 1.5% PP-MMT

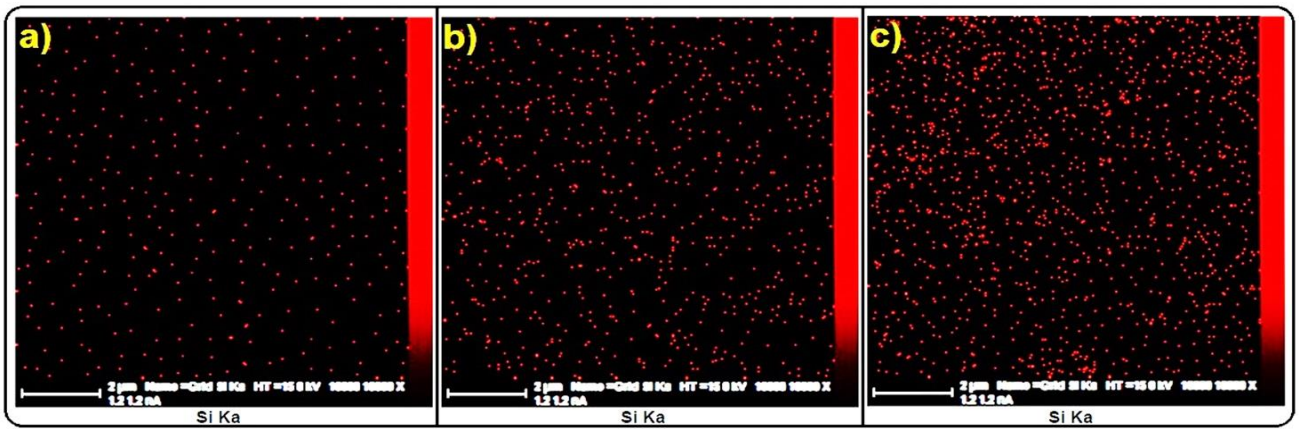

Fig. 4: Dispersion of PP-MMT in matrix: (a) EP / 0.5% PP-MMT (b) EP / 1% PP-MMT (c) EP / 1.5% PP-MMT

With increasing the PP-MMT content in the matrix (5.62° (*d*-spacing = 19.21 Å) for EP/0.5% PP-MMT, 5.43° (*d*-spacing = 20.16 Å) for EP/1% PP-MMT, and 5.2° (*d*-spacing = 21.44 Å) for EP/1.5% PP-MMT), the peak is seen at 2θ lower values; furthermore, the intensity and *d*-spacing increase. The penetration of EP polymer chains into MMT galleries is the reason for these changes in XRD pattems [45,46]. The morphology of EP and EP/1.5% PP-MMT was evaluated using SEM images (see Fig. 3). The SEM images (Fig. 3a-b) show that the surface of EP is very smooth. Unlike EP, the nanocomposite has a rough surface, and a plate structure is observed due to the presence of PP-MMT (see Fig. 3c-d). Also, the red points in Fig. 4 (SEM-EDX mapping) are Si atoms, showing the distribution of PP-MMT in the nanocomposites.

The results obtained from the potentiodynamic polarization curve are presented in Fig. 5 and Table 2. The values of E_{corr} and I_{corr} for EP were -0.629 V and 9.642×10^{-7} µA, respectively,

Table 2: Polarization parameters of samples immersed in 3.5 wt. % NaCl solution

Samples	E_{corr} (V)	I_{corr} (μA.cm^{-2})	β_a (V/dec)	β_c (V/dec)	C.R (mm/year)	R_p (Ω.cm^2)	IE (%)
EP	-0.629	9.642×10^{-7}	0.204	0. 064	1.139×10^{-2}	2.949×10^{3}	-
EP/0.5% PP-MMT	-0.601	7.863×10^{-7}	0.269	0.077	9.34×10^{-3}	5.64×10^{3}	18.45
EP/1% PP-MMT	-0.552	4.697×10^{-7}	0.324	0.091	5.539×10^{-3}	1.389×10^{4}	51.28
EP/1.5% PP-MMT	-0.549	1.238×10^{-7}	0.212	0.086	1.44×10^{-3}	3.321×10^{4}	87.16

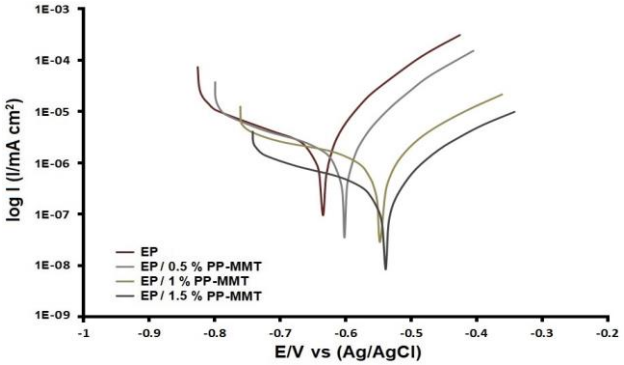

Fig. 5: The polarization curves of samples immersed in 3.5 wt. % NaCl solution

which confirmed that this coating was susceptible to corrosion. According to the results, it is clear that the nanocomposite coatings showed a completely different corrosion resistance from EP coatings [47,48]. With increasing PP-MMT content in the matrix, E_{corr} moved to higher-level values while I_{corr} decreased. The reduction of I_{corr} and the increase of E_{corr} can be ascribed to the anodic inhibition mechanism, although for coatings containing PP-MMT nanocompounds, both anodic and cathodic segments in Fig. declined to lower quantities of current densities, representing mixed (anodic-cathodic) corrosion inhibition. Steel surfaces coated with EP/1.5% PP-MMT with more positive values of E_{corr} (-0.549 V) and a significant decrease in I_{corr} (1.238×10^{-7} μA), as well as an increase in R_p (3.321×10^{4} Ω.cm^2) and a decrease in C.R (1.460×10^{-3} mm/year) showed better anti-corrosion performance than other samples. The anti-corrosion performance of the nanocomposite coatings can be explained by the synergistic influence of MMT and PP compounds [49,50]. The sheet- or plate-like structure of MMT in the matrix of EP elongates the penetration path of corrosive ions and acts as a physical barrier against aggressive species. The MMT also reacts with hydroxyl ions in the cathodic region, producing insoluble compounds and preventing oxygen from reaching the cathodic region. On the other hand, PP has many bioactive compounds including flavonoids, lignin, phenolic acid, amino acids (glutamic acid, glycine, valine), and polysaccharide [51,52]. These organic compounds contain benzene rings, heteroatoms (carbon, oxygen and nitrogen), and carbonyl groups that share their free electron pairs with the empty orbital of iron atoms of the metal surface and are absorbed by a chemisorption mechanism on the metal surface [51]. This leads to the creation of a barrier layer at the metal/coating interface and blocks anodic regions. Also, PP repels water and increases corrosion resistance because it has different amino acids that have hydrophobic side chains [53,54].

Fig. 6 shows the corrosion inhibitory behavior of coated plates by the salt spray test after 400 h. Rusts, blisters, and acute corrosion products are observed on the EP coating indicating that the EP coating has poor corrosion resistance. The results show that the corrosion around the scratch decreases with increasing PP-MMT content. Meanwhile, the nanocomposite coating contains 1.5 *wt.* % PP-MMT, showing only very few rust spots. This proves the corrosion resistance due to the presence of PP-MMT.

Fig. 7 illustrates the adhesion strength, coefficient of friction, and the wear rate of coatings. The adhesion strength of EP, EP/0.5% PP-MMT, EP/1% PP-MMT, and EP/1.5% PP-MMT were 7.1, 7.2, 7.8, and 8.2 MPa, respectively. It can be seen that with increasing the nanoparticle content, the adhesion property improves due to the release of residual stress inside the coating by PP-MMT. Fig. 7b shows the coefficient of friction increasing rapidly, which is due to the smooth surfaces of all coatings in the first stage. As the results show, that with increasing PP-MMT content, the coefficient of friction is stabilized at a less value. During friction due to the presence of PP-MMT, the surface morphology gradually deformed, increasing the surface roughness while decreasing the mechanical contact area [55]. The wear rate of the coatings decreased with increasing PP-MMT content in the matrix (see Fig. 7c). The wear rates of EP, EP/0.5% PP-MMT, EP/1% PP-MMT, and

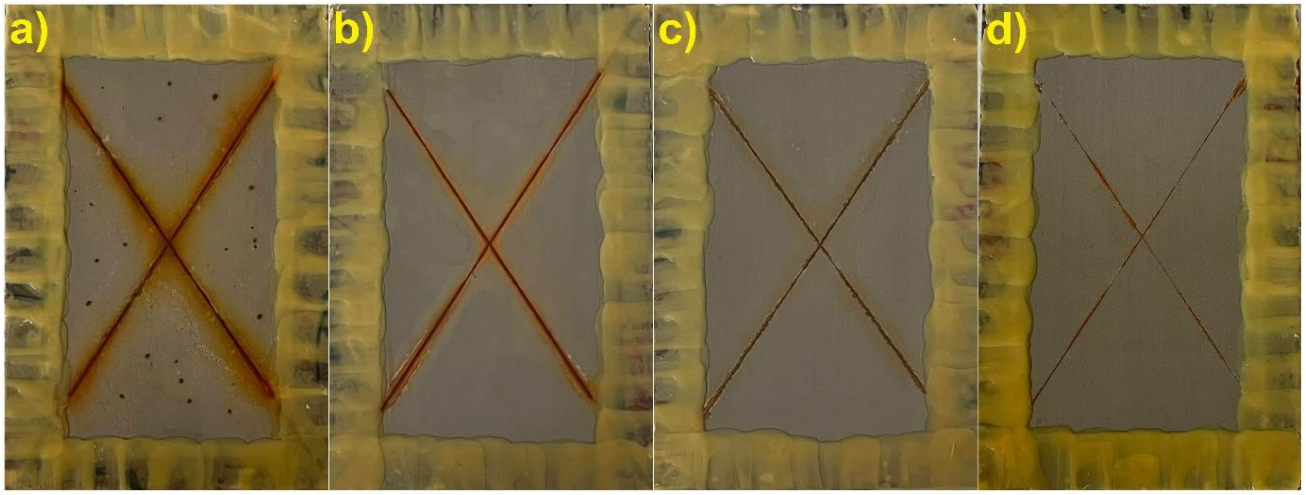

Fig. 6: Images of coatings after 400 h exposure to salt spray test: (a) EP (b) EP / 0.5% PP-MMT (c) EP / 1% PP-MMT (d) EP / 1.5% PP-MMT

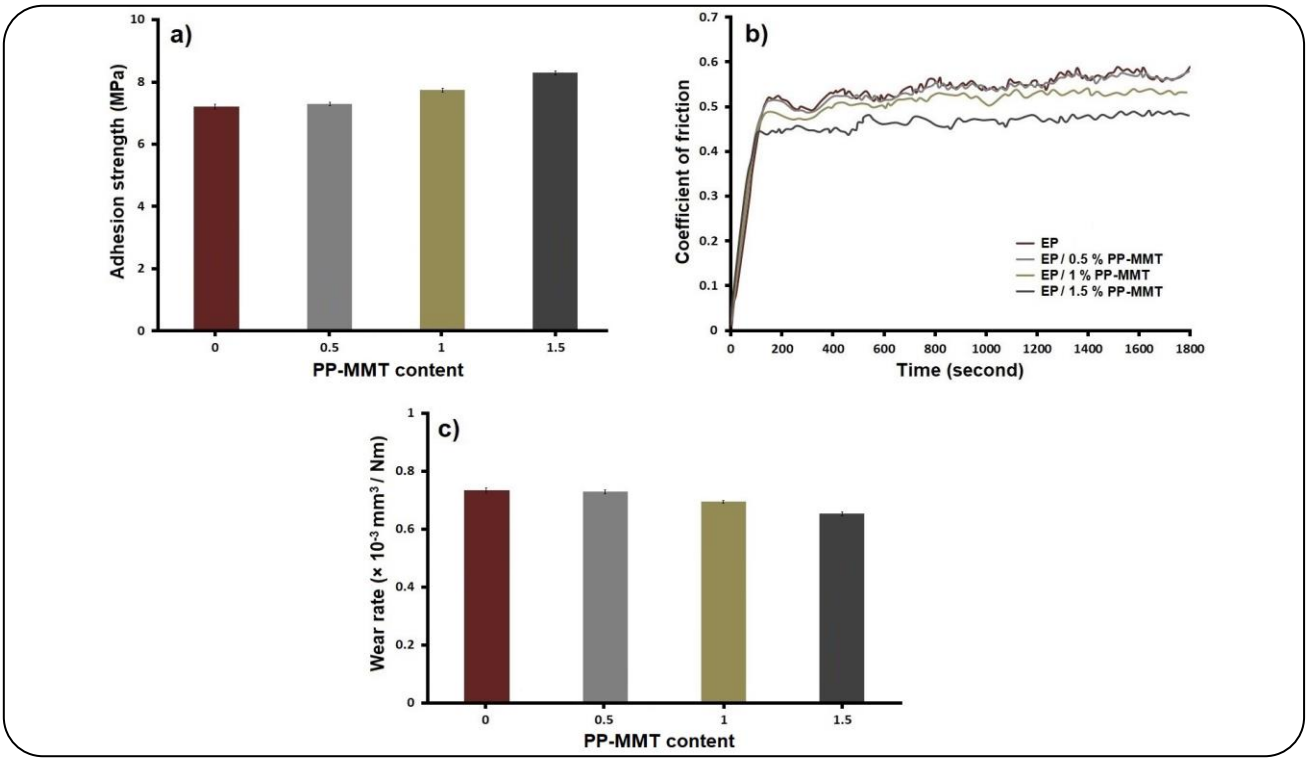

Fig. 7: (a) Adhesion strength, (b) coefficient of friction, and (c) wear rate of samples

EP/1.5% PP-MMT were 0.734, 0.722, 0.692, and 0.652 respectively. The wear rate of coatings decreases with increasing PP-MMT content in the matrix because, during the friction process, PP-MMT mixes with EP to form a sintered layer [56].

Table 3 shows the tensile test results of the samples. The results show that the presence of PP-MMT in the matrix increases the strength and Young's modulus, the behavior of which has been reported in the literature [57,58]. As the XRD and SEM-EDX mapping results of nanocomposites showed, the polymer chains were able to penetrate into the MMT galleries and a uniform distribution of nanoparticles was obtained in the matrix. Hence, many stress damping reduction sites are created in the matrix, and the nanocomposite can easily eliminate the stress without destruction.

Table 3: Tensile strength results of samples containing different amounts of PP-MMT

Samples	Strength(MPa)	Young's modulus (MPa)
EP	4.6 ± 0.1	397 ± 2
EP/0.5% PP-MMT	4.9 ± 0.1	412 ± 1
EP/1% PP-MMT	5.4 ± 0.1	460 ± 1
EP/1.5% PP-MMT	5.9 ± 0.1	523 ± 1

Table 4: Antimicrobial activity of samples

Microorganism	DD	MIC	MBC
Bacillus subtilis	-[a] 6[b]	-[a] 500[b]	-[a] 1000[b]
Staphylococcus epidermidis	-[a] 4[b]	-[a] 500[b]	-[a] 1000[b]
Escherichia coli	-[a] 3[b]	-[a] 1000[b]	-[a] 2000[b]
Shigella dysenteriae	-[a] 2[b]	-[a] 1000[b]	-[a] 2000[b]

Note:

* DD: Disk diffusion method, inhibition zones in diameter (mm) around the impregnated disk.

** DD: 600 µg per well

*** Concentrations of MIC and MBC as µg/mL

**** [a]EP, [b]EP/1.5% PP-MMT

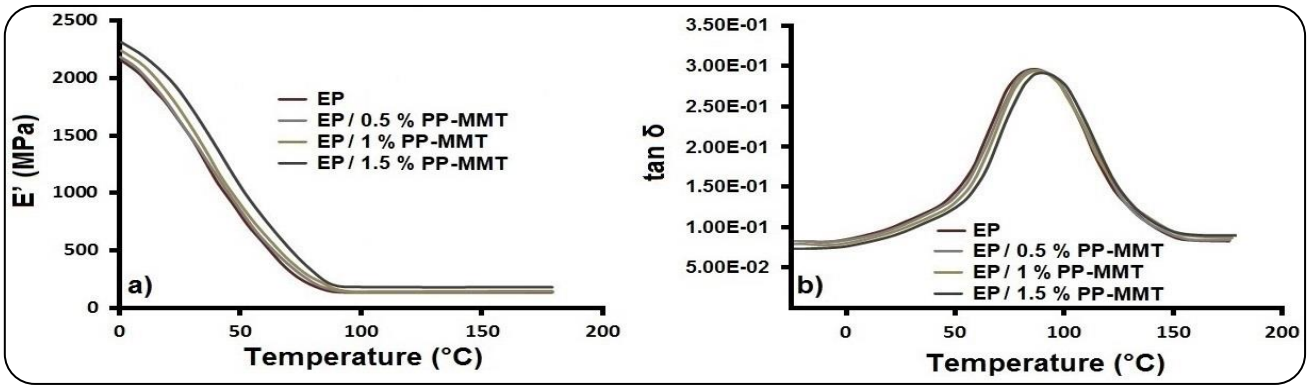

Fig. 8: Dynamic-mechanical

Fig. 8 shows the dynamic-mechanical studies of the samples. The results show that (Fig. 8a), EP presented a high E' of ۲۱۷۰ MPa at 0 °C. Due to the increased mobility of macromolecules with increasing temperature, the E' of EP decreases. With the addition of PP-MMT, the storage modulus is increased. As can be seen, this increase continues at higher temperatures. It can be said that this behavior at higher temperatures is due to the low content of PP-MMT, which can slightly affect the viscosity of macromolecules at higher temperatures. Storage modules were observed for EP/0.5% PP-MMT, EP/1% PP-MMT, and EP/1.5% PP-MMT 2180, 2245, and 2350 MPa, respectively. It can be seen that with the addition of PP-MMT, the position, and intensity of the tan δ peak change (Fig. 8b). The shift of the tan δ peak to higher temperatures (0.3 °C for EP/0.5% PP-MMT, 1 °C for EP/1% PP-MMT, and 2.5 °C for EP/1.5% PP-MMT) indicates the limitation polymer chains in the structure [59]. Also, the T_g of EP, EP/0.5% PP-MMT, EP/1% PP-MMT, and EP/1.5% PP-MMT were 90 °C, 90.3 °C, 91 °C, and 92.5 °C, respectively. In addition, a decrease in tan δ is due to the interactions and penetration of macromolecules into the MMT galleries (see XRD discussion of nanocomposite).

Behavior of samples: (a) E', (b) tanδ curves

In this study, the antimicrobial properties of EP and EP/1.5% PP-MMT against two types of gram-positive bacteria (*Bacillus subtilis* (ATCC 6633) and *Staphylococcus epidermidis* (CIP 81.55))

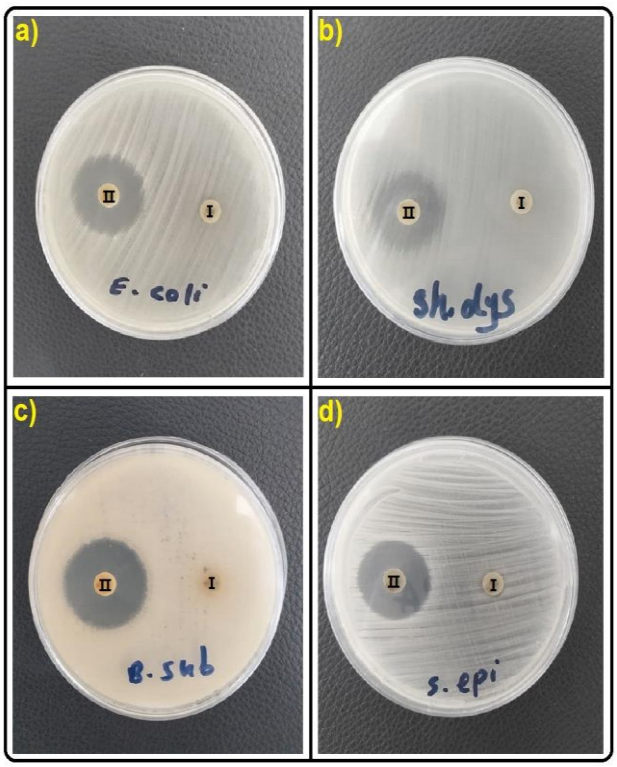

Fig. 9: Antibacterial activity of (I) EP and (II) EP / 1.5% PP-MMT: (a) Escherichia coli, (b) Shigella dysenteriae, (c) Bacillus subtilis, and (d) Staphylococcus epidermidis

and two types of gram-negative bacteria (*Escherichia coli* (ATCC 25922) and *Shigella dysenteriae* (PTCC 1188)) were investigated (see Table 4 and Fig. 9). The results show that EP does not affect gram-positive and gram-negative bacteria. The formation of inhibition zones by EP/1.5% PP-MMT is due to the presence of PP in the structure. PP contains proteins, amino acids, lipids, flavonoids, phenolic acids, nucleic acids, saccharides, vitamin D, and other nutrients, which is why it has immune-enhancing, anti-inflammatory, and anti-cancer, antioxidant, and antibacterial effects [43,60-62]. Phenolic compounds have the ability to suppress membrane perturbation, reduction of host ligand adhesion, and neutralize bacterial toxins [63-65]. Hence, PP was known as a medicinal plant in the past and was used in some countries such as China [52,66]. The results show that PP has a greater effect on gram-positive bacteria, which is owing to the difference in the structure of the bacterial cell wall [67-69]. The cell wall of gram-positive bacteria is simple and porous, so it is easier to penetrate, but the structure of the cell wall of gram-negative bacteria is complex and less porous [37].

CONCLUSIONS

To sum up, we swollen Na^+-MMT and successfully added PP to the structure, and the results of FT-IR, XRD, SEM, and TEM confirmed this modification. The results showed that after modification of Na^+-MMT, 2θ changes and the *d*-spacing increases, which was owing to the presence of PP in the interlayer space of MMT. According to X-ray patterns, polymer chains were able to easily penetrate MMT galleries, and also with increasing the PP-MMT content in the matrix, the peak intensity and *d*-spacing increased. Also, by an increase of PP-MMT in matrix, E', T_g, Young's modulus, corrosion resistance, and adhesion strength were increased. The antimicrobial study showed that PP-MMT even in the content used in this study (up to 1.5*wt.* %) could have an inhibitory effect on bacteria. It is very important to use environmentally friendly corrosion inhibitors because they are non-toxic and do not harm the environment. Many green inhibitors are highly capable of controlling steel corrosion, but are not fully available. According to the properties of PP-MMT, it can be said that PP is a suitable candidate in the field of anti-corrosion and antimicrobial due to its low cost, availability and compatibility with the environment.

Received : Nov.21, 2022 ; Accepted : Feb.06, 2023

REFERENCES

[1] Farhadian A., Varfolomeev M.A., Rahimi A., Mendgaziev R.I., Semenov A.P., Stoporev A.S., Vinogradova S.S., Karwt R., Kelland M.A., Gas Hydrate and Corrosion Inhibition Performance of the Newly Synthesized Polyurethanes: Potential Dual Function Inhibitors, *Energy Fuels.*, **35(7)**: 6113-6124 (2021).

[2] Edraki M, Sheydaei M., Zaarei D., Salmasifar A., Azizi B., Protective Nanocomposite Coating Based on Ginger Modified Clay and Polyurethane: Preparation, Characterization and Evaluation Anti-Corrosion and Mechanical Properties, *Polym. Sci. Ser. B.*, **64**: 756-764 (2022).

[3] Ameri E., Jafari H., Rezaeevala M., Vakili M.H., Mokhtarian N., Synthesized Schiff Base Acted as Eco-Friendly Inhibitor for Mild Steel in 1N H_2SO_4, *Chem. Rev. Lett.*, **5(2)**:119-126 (2022).

[4] Barroso G., Li Q., Bordia, R.K., Motz G., Polymeric and Ceramic Silicon-Based Coatings–A Review, *J. Mater. Chem. A.*, **7(5)**: 1936-1963 (2019).

[5] May C.A., "Epoxy Resins, Chemistry and Technology", 2nd ed., Marcel Dekker, New York, Basel (1988).

[6] Park S.J., Jin F.L., Nicolais L., Nicolais, A. Borzacchiello (Eds.), "Wiley Encyclopedia of Composites", John Wiley & Sons (2011).

[7] Jin F.L., Li X., Park S.J., Synthesis and Application of Epoxy Resins: A Review, *J. Ind. Eng. Chem.*, **29**: 1-11(2015).

[8] De Farias M.A., Coelho L.A.F., Pezzin S.H., Hybrid Nanocomposites Based on Epoxy/Silsesquioxanes Matrices Reinforced with Multi-Walled Carbon Nanotubes, *Mater. Res.*, **18**: 1304-1312 (2015).

[9] Zhang Y., Yu B., Wang B., Liew K.M., Song L., Wang C., Hu Y., Highly Effective P–P Synergy of a Novel DOPO-Based Flame Retardant for Epoxy Resin, *Ind. Eng. Chem. Res.*, **56(5)**: 1245-1255 (2017).

[10] Sukanto H., Raharjo W.W., Ariawan D., TriyonoJ., Kaavesina M., Epoxy Resins Thermosetting for Mechanical Engineering, *Open Eng.*, **11(1)**: 797-814 (2021).

[11] Tang S., Wachtendorf V., Klack P., Qian L., Dong Y., Schartel B., Enhanced Flame-Retardant Effect of a Montmorillonite/Phosphaphenanthrene Compound in an Epoxy Thermoset, *RSC Adv.*, **7(2)**: 720-728 (2017).

[12] Sheydaei M., Jabari M., Ali-Asgari Dehaghi H.R., Synthesis and Characterization of Ethylene-Xylene-Based Polysulfide Block-Copolymers Using the Interfacial Polymerization Method, *J. Sulfur Chem.*, **37(6)**: 646-655 (2016).

[13] Sheydaei M., Edraki M., Alinia-Ahandani E., Nezhadghaffar-Borhani E., Poly (Ethylene Disulfide)/Carbon Fiber Composites: Cure and Effect of Fiber Content on Mechanical and Thermal Properties, *J. Sulfur Chem.*, **42(6)**: 614-627 (2021).

[14] Sheydaei M., Edraki M., Javanbakht S., Alinia-Ahandani E., Soleimani M., Zerafatkhah A., Poly (Butylene Disulfide) and Poly (Butylene Tetrasulfide): Synthesis, Cure and Investigation of Polymerization Yield and Effect of Sulfur Content on Mechanical and Thermophysical Properties, *Phosphorus Sulfur Silicon Relat. Elem.*, **196(6)**: 578-584 (2021).

[15] Sheydaei M., Edraki M., Mousazadeh Moghaddampour I., Alinia-Ahandani E., Poly (Butylene Trisulfide)/SiO_2 Nanocomposites: Cure and Effect of SiO_2 Content on Mechanical and Thermophysical Properties, *J. Sulfur Chem.*, **43(4)**: 413-425 (2022).

[16] Sheydaei M., Sodium Sulfide-Based Polysulfide Polymers: Synthesis, Cure, Thermal and Mechanical Properties, *J. Sulfur Chem.*, **43(6)**: 643-654 (2022).

[17] Sheydaei M., Edraki M., Mousazadeh Moghaddampour I., Poly (*p*-Xylene Trisulfide): Synthesis, Curing and Investigation of Mechanical and Thermal Properties, *Polym. Sci. Ser. B.*, **64(4)**: 464-469 (2022).

[18] Sheydaei M., Talebi S., Salami-Kalajahi M., Synthesis, Characterization, Curing, Thermophysical and Mechanical Properties of Ethylene Dichloride-Based Polysulfide Polymers, *J. Macromol. Sci., Part A: Pure Appl. Chem.*, **58(5)**: 344-352(2021).

[19] Sheydaei M., Talebi S., Salami-Kalajahi M., Synthesis of Ethylene Dichloride-Based Polysulfide Polymers: Investigation of Polymerization Yield and Effect of Sulfur Content on Solubility and Flexibility, *J. Sulfur Chem.*, **42(1)**: 67-82 (2021).

[20] Edraki M., Sheydaei M., Alinia-Ahandani E., Nezhadghaffar-Borhani E., Polyvinyl Chloride: Chemical Modification and Investigation of Structural and Thermal Properties, *J. Sulfur Chem.*, **42(4)**: 397-409 (2021).

[21] Hsissou R., Abbout S., Seghiri R., Rehioui M., Berisha A., Erramli H., Assouag M., Elharfi A., Evaluation of Corrosion Inhibition Performance of Phosphorus Polymer for Carbon Steel in [1 M] HCl: Computational Studies (DFT, MC and MD Simulations), *J. Mater. Res. Technol.*, **9(3)**: 2691-2703 (2020).

[22] Saravanan P., Jayamoorthy K., Kumar S.A., Design and Characterization of Non-Toxic Nano-Hybrid Coatings for Corrosion and Fouling Resistance, *J. Sci.: Adv. Mater. Devices.*, **1(3)**: 367-378 (2016).

[23] Edraki M., Mousazadeh Moghaddampour I., Banimahd Keivani M., Sheydaei M., Characterization and Antimicrobial Properties of Matcha Green Tea, *Chem. Rev. Lett.*, **5(1)**: 76-82 (2022).

[24] Edraki M., Mousazadeh Moghaddampour I., Alinia-Ahandani E., banimahd keivani M., Sheydaei M., Ginger Intercalated Sodium Montmorillonite Nano Clay: Assembly, Characterization, and Investigation Antimicrobial Properties, *Chem. Rev. Lett.*, **4(2)**: 120-129 (2021).

[25] Ahamed M.I., Prasad R., "Advanced Antimicrobial Materials and Applications", Springer, Singapore (2021).

[26] Aroh Oyibo A., Arthur D., Danzarami D., The use of Strawberry and Arabic Gum Blend as an Inhibitor for the Corrosion of Aluminium in an Acidic Medium, *Chem. Rev. Lett.*, **2(2)**: 69-75 (2019).

[27] Williams C.G., Atmospheric Layering During Peak Pine Pollen Season, *Grana*., **59(6)**: 466-475 (2020).

[28] Luo Y., Yin P., Wu G., Zhang L., Ma G., Wang J., Sun X., Bu G., Porous Carbon Sphere Decorated with Co/Ni Nanoparticles for Strong and Broadband Electromagnetic Dissipation, *Carbon*., **197**: 389-399 (2022).

[29] Cheng Y., Quan W., Qu T., He Y., Wang Z., Zeng M., Qin F., Chen J., He Z., Effects of ^{60}Co-Irradiation and Superfine Grinding Wall Disruption Pretreatment on Phenolic Compounds in Pine (*Pinus yunnanensis*) Pollen and Its Antioxidant and α-Glucosidase-Inhibiting Activities, *Food Chem*., **345**: 128808 (2021).

[30] Dehghani A., Bahlakeh G., Ramezanzadeh B., Mofidabadi A.H.J., Mostafatabar A.H., Benzimidazole Loaded β-cyclodextrin as a Novel Anti-Corrosion System; Coupled Experimental/Computational Assessments, *J. Colloid Interface Sci*., **603**: 716-727 (2021).

[31] Dong Y., Wang F., Zhou, Q., Protective Behaviors of 2-Mercaptobenzothiazole Intercalated Zn–Al-Layered Double Hydroxide Coating, *J. Coat. Technol. Res*., **11(5)**: 793-803 (2014).

[32] Jayrajsinh S., Shankar G., Agrawal Y.K., Bakre L., Montmorillonite Nanoclay as a Multifaceted Drug-Delivery Carrier: A Review, *J. Drug Deliv. Sci. Technol.*, **39**: 200-209 (2017).

[33] Rajendran D., Sasilatha T., Rajendran S.S., Al-Hashem A., Lačnjevac Č., Singh G., Inhibition of Corrosion of Mild Steel Hull Plates Immersed in Natural Sea Water by Sandalwood Oil Extract of Some Natural Products, *Mater. Prot*., **63(1)**: 23-36 (2022).

[34] Zhang X., Noël-Hermes N., Ferrari G., Hoogeland M., Localized Corrosion of Mooring Chain Steel in Seawater, *Corros. Mater. Degrad*., **3(1)**: 53-74 (2022).

[35] Ricky E., Lugwisha E., Philip J., Corrosion Inhibition of Mild Steel in Seawater by 2, 4, 6-Triamino-3-Pentadecylphenyl Acetate Derived From Cashew Nut Shell Liquid, *Tanz. J. Sci*., **47(1)**: 112-122 (2021).

[36] Hajiyan Pour F., Rajabi M., Behpour M., Jafari Y., Investigation of Corrosion Protection Performance of Epoxy Coatings Modified by ZnO-Cr_2O_3 Nanocomposites on Mild Steel Surfaces, *J. Appl. Chem*., **13(49)**: 45-52 (2018).

[37] Sheydaei M., Pouraman V., Alinia-Ahandani E., Shahbazi-Ganjgah S., PVCS/GO Nanocomposites: Investigation of Thermophysical, Mechanical and Antimicrobial Properties, *J. Sulfur Chem*., **43(4)**: 376-390 (2022).

[38] Nasrabadi H.S., Kalaee M.R., Abdouss M., Sheydaei M., Mazinani S., New Role of Layered Silicates as Phase Transfer Catalyst for In Situ Polymerization of Poly(Ethylenetetrasulfide) Nanocomposite, *J. Inorg. Organomet. Polym*., **23**: 950-957 (2013).

[39] Mistry B.D., "A Handbook of Spectroscopic Data Chemistry", Oxford Book Company: Jaipur (2009).

[40] Socrates G., "Infrared and Raman Characteristic Group Frequencies", 3rd ed. Wiley, New York (2001).

[41] de Almeida J.C., de Barros A., Mazali I.O., Ferreira M., Influence of Gold Nanostructures Incorporated into Sodium Montmorillonite Clay Based on LbL Films for Detection of Metal Traces Ions, *Appl. Surf. Sci.*, **507**: 144972 (2020).

[42] Lei Y., Zhou Q., Zhang Y.L., Chen J.B., Sun S.Q., Noda I., Studies on the Preparation and Properties of Sol-Gel Molecularly Imprint Polymer Based on Tetraethoxysilane for Recognizing Sulphonamides, *J. Mol. Struct*., **974(1-3)**: 88-93 (2010).

[43] Xu X.L., Zheng Y.Z., Chen X.C., Zhu F.L., Miao X.Q., Identification of Cattail Pollen, Pine Pollen and Bee Pollen by Fourier Transform Infrared Spectroscopy and Two-Dimensional Correlation Infrared Spectroscopy, *J. Mol. Struct.*, **1167**: 78-81 (2018).

[44] Izadi M., Shahrabi T., Mohammadi I., Ramezanzadeh B., Synthesis of Impregnated Na^+-Montmorillonite as an Eco-Friendly Inhibitive Carrier and Its Subsequent Protective Effect on Silane Coated Mild Steel, *Prog. Org. Coat.*, **135**: 135-147 (2019).

[45] Heidarian M., Shishesaz M.R., Kassiriha S.M., Nematollahi M., Characterization of Structure and Corrosion Resistivity of Polyurethane/Organoclay Nanocomposite Coatings Prepared Through an Ultrasonication Assisted Process, *Prog. Org. Coat*., **68(3)**: 180-188 (2010).

[46] Ashhari S., Sarabi A.A., Kasiriha S.M., Zaarei D., Aliphatic Polyurethane–Montmorillonite Nanocomposite Coatings: Preparation, Characterization, and Anticorrosive Properties, *J. Appl. Polym. Sci.*, **119(1)**: 523-529 (2011).

[47] Chen Y., Bai W., Chen J., Chen X., Wei F., Jian R., Zheng X., Xu, Y., In-Situ Intercalation of Montmorillonite/Urushiol Titanium Polymer Nanocomposite for Anti-Corrosion and Anti-Aging of Epoxy Coatings, *Prog. Org. Coat.*, **165**: 106738 (2022).

[48] Razizadeh M., Mahdavian M., Ramezanzadeh B., Alibakhshi E., Jamali S., Synthesis of Hybrid Organic–Inorganic Inhibitive Pigment Based on Basil Extract and Zinc Cation for Application in Protective Construction Coatings, *Constr. Build. Mater.*, **287**: 123034 (2021).

[49] Edraki M., Zaarei D., Azole Derivatives Embedded in Montmorillonite Clay Nanocarriers as Corrosion Inhibitors of Mild Steel, *Int. J. Miner. Metall. Mater*., **26(1)**: 86-97 (2019).

[50] Wang X., Ren S.F., Zhang D.X., Jiang H., Gu Y., Inhibitory Effect of Pinus Massoniana Needle Extract on Corrosion of Q235 Steel in Hydrochloric Acid Medium, *Int. J. Electrochem. Sci.*, **13**: 9888-9904 (2018).

[51] Hamadi L., Mansouri S., Oulmi K., Kareche A., The Use of Amino Acids as Corrosion Inhibitors for Metals: A Review, *Egypt. J. Pet*., **27(4)**: 1157-1165 (2018).

[52] Wang Y.M., Wang H.J., Zhang Z.Y., Analysis of Pine Pollen by Using FTIR, SEM and Energy-Dispersive X-ray Analysis, *Guang Pu Xue Yu Guang Pu Fen Xi*., **25(11)**: 1797-1800 (2005).

[53] Ala'a B., Salman T.A., Corrosion Inhibition of Carbon Steel in Saline Solution Using Amino Acids, *Int. J. Pharm. Sci. Rev. Res*., **40**(1): 182-190 (2016).

[54] Ma F., Chen J.B., Wu X.X., Zhou Q., Sun S.Q., Rapid Discrimination of Panax Notogeinseng of Different Grades by FT-IR and 2DCOS-IR, *J. Mol. Struct*., **1124**: 131-137 (2016).

[55] Ye Y., Zhang D., Li J., Liu T., Pu J., Zhao H., Wang L., One-Step Synthesis of Superhydrophobic Polyhedral Oligomeric Silsesquioxane-Graphene Oxide and its Application in Anti-Corrosion and Anti-Wear Fields, *Corros. Sci.*, **147**: 9-21 (2019).

[56] Österle W., Dmitriev A.I., Wetzel B., Zhang G., Häusler I., Jim B.C., The Role of Carbon Fibers and Silica Nanoparticles on Friction and Wear Reduction of an Advanced Polymer Matrix Composite, *Mater. Design*., **93**: 474-484 (2016).

[57] Wang M., Fan X., Thitsartarn W., He C., Rheological and Mechanical Properties of Epoxy/Clay Nanocomposites with Enhanced Tensile and Fracture Toughnesses, *Polymer*., **58**: 43-52 (2015).

[58] Xu Y., Van Hoa S., Mechanical Properties of Carbon Fiber Reinforced Epoxy/Clay Nanocomposites, *Compos. Sci. Technol*., **68(3-4)**: 854-861 (2008).

[59] Allahbakhsh A., Khodabadi F.N., Hosseini F.S., Haghighi A.H., 3-Aminopropyltriethoxysilane-Functionalized Rice Husk and Rice Husk Ash Reinforced Polyamide 6/Graphene Oxide Sustainable Nanocomposites, *Eur. Polym. J.*, **94**: 417-430 (2017).

[60] Lee K.H., Choi E.M., Effect of Pine Pollen Extract on Experimental Chronic Arthritis, *Phytother. Res*., **23(5)**: 651-657 (2009).

[61] Hoai N.T., Duc, H.V., Orav, A., Raal, A., Selective Cytotoxic Action of Scots Pine (*Pinus Sylvestris L.*) Needles Extract in Human Cancer Cell Lines, *Pharmacogn. Mag*., **11(2)**: S290-295 (2015).

[62] Daglia M., Polyphenols as Antimicrobial Agents, *Curr. Opin. Biotechnol*., **23(2)**:174-181 (2012).

[63] Aras A., Bursal E., Alan Y., Turkan F., Alkan H., Kılıç, Ö., Polyphenolic Content, Antioxidant Potential and Antimicrobial Activity of *Satureja Boissieri*, *Iran. J. Chem. Chem. Eng. (IJCCE)*, **37(6)**: 209-219 (2018).

[64] Ebrahimi Anaraki P., Aboee-Mehrizi F., Dehghani Ashkezary M., Sedighi S., Chemical Composition and Biological Activities of Essential Oil and Methanol Extract of Teucrium Scordium, *Iran. J. Chem. Chem. Eng.(IJCCE)*, **39(2)**: 207-215 (2020).

[65] Nakhaee Moghadam M., Movaffagh J., Fazli Bazzaz B.S., Azizzadeh M., Jamshidi A., Encapsulation of Zataria Multiflora Essential oil in Saccharomyces Cerevisiae: Sensory Evaluation and Antibacterial Activity in Commercial Soup, *Iran. J. Chem. Chem. Eng.(IJCCE)*, **39(2)**: 233-242 (2020).

[66] Lee K.H., Kim A.J., Choi E.M., Antioxidant and Antiinflammatory Activity of Pine Pollen Extract in Vitro, *Phytother. Res*., **23(1)**: 41-48 (2009).

[67] Safaeian Laein S., Salari A., Shahsavani D., Haghishani H., Evaluation of Antibacterial and Antioxidant Activities of Essential Oil of Lime (*Citrus Aurantifolia*) Pomace Powder, *Iran. J. Chem. Chem. Eng.(IJCCE)*, **40(3)**: 832-840 (2021).

[68] Momeni M., Asadi S., Shanbedi, M., Antimicrobial Effect of Silver Nanoparticles Synthesized with Bougainvillea Glabra Extract on *Staphylococcus Aureus* and *Escherichia Coli*, *Iran. J. Chem. Chem. Eng. (IJCCE)*, **40(2)**: 395-405 (2021).

[69] Bahrin L.G., Apostu M.O., Birsa L.M., Stefan M., The Antibacterial Properties of Sulfur Containing Flavonoids, *Bioorg. Med. Chem. Lett*., **24(10)**: 2315-2318 (2014).